Chinese Journal of Natural Medicines

***Apocynum venetum* leaf extract ameliorates postmenopausal osteoporosis by inhibiting RANKL-induced osteoclastogenesis**

Yongyan Chen, Shuo Gao, Yunqing Xu, Jiebo Chen, Congwei Liu, Zhenwu Wang, Zhiping Zeng, Ting Lin, Hu Zhou

Citation: Yongyan Chen, Shuo Gao, Yunqing Xu, Jiebo Chen, Congwei Liu, Zhenwu Wang, Zhiping Zeng, Ting Lin, Hu Zhou, *Apocynum venetum* leaf extract ameliorates postmenopausal osteoporosis by inhibiting RANKL-induced osteoclastogenesis, Chinese Journal of Natural Medicines, 2026, 24(6), 710-719. doi: 10.1016/S1875-5364(26)61186-7.

View online: https://doi.org/10.1016/S1875-5364(26)61186-7

Related articles that may interest you

Ethanol extract of Cyathulae Radix inhibits osteoclast differentiation and bone loss

Chinese Journal of Natural Medicines. 2024, 22(3), 212-223 https://doi.org/10.1016/S1875-5364(24)60596-0

Study on the action mechanism of *Wuling* Powder on treating osteoporosis based on network pharmacology

Chinese Journal of Natural Medicines. 2021, 19(1), 28-35 https://doi.org/10.1016/S1875-5364(21)60003-1

Mulberry leaf flavonoids activate BAT and induce browning of WAT to improve type 2 diabetes *via* regulating the AMPK/SIRT1/PGC-1 α signaling pathway

Chinese Journal of Natural Medicines. 2023, 21(11), 812-829 https://doi.org/10.1016/S1875-5364(23)60481-9

Artemisia kruhsiana leaf extract induces autophagic cell death in human prostate cancer cells

Chinese Journal of Natural Medicines. 2021, 19(2), 134-142 https://doi.org/10.1016/S1875-5364(21)60014-6

Rapid identification of stigmastane-type steroid saponins from *Vernonia amygdalina* leaf based on α-glucosidase inhibiting activity and molecular networking

Chinese Journal of Natural Medicines. 2022, 20(11), 846-853 https://doi.org/10.1016/S1875-5364(22)60235-8

Effective fraction from Simiao Wan prevents hepatic insulin resistant by inhibition of lipolysis *via* AMPK activation

Chinese Journal of Natural Medicines. 2022, 20(3), 161-176 https://doi.org/10.1016/S1875-5364(21)60115-2

Wechat

Chinese Journal of Natural Medicines 24 (2026) 710-719

Contents lists available at ScienceDirect

Chinese Journal of Natural Medicines

journal homepage: www.cjnmcpu.com/

Original article

Apocynum venetum leaf extract ameliorates postmenopausal osteoporosis by inhibiting RANKL-induced osteoclastogenesis

Yongyan Chen[a,Δ], Shuo Gao[a,Δ], Yunqing Xu[a], Jiebo Chen[a], Congwei Liu[a,b], Zhenwu Wang[a,b], Zhiping Zeng[a,b], Ting Lin[a,*], Hu Zhou[a,b,*]

[a] *School of Pharmaceutical Sciences, Fujian Provincial Key Laboratory of Innovative Drug Target Research, Xiamen University, Xiamen 361102, China*
[b] *High Throughput Drug Screening Platform, Xiamen University, Xiamen 361102, China*

ARTICLE INFO

Article history:
Received 19 August 2025
Revised 23 December 2025
Accepted 2 January 2026
Available online 20 June 2026

Keywords:
Apocynum venetum leaf
AVL fraction
Postmenopausal osteoporosis
Osteoclastogenesis
RANKL

ABSTRACT

Identifying novel therapeutic efficacies of traditional Chinese medicine (TCM) and their underlying mechanisms is essential for TCM modernization and development. *Apocynum venetum* leaf (AVL) is used both as an antihypertensive medicine and as a food. Whether AVL extract possesses additional therapeutic efficacies remains to be investigated. Here, we examined the potential effect of AVL extract on ameliorating postmenopausal osteoporosis (PMO) and identified the effective fractions and underlying mechanisms of its efficacy. We found that the total extract of AVL substantially relieved osteoporosis symptoms in both mouse and rat ovariectomized models. Moreover, the AVL-95% fraction, accounting for only about 2% of the total extract, exhibited a therapeutic effect on osteoporosis comparable to that of the total extract. Notably, the AVL-95% fraction improved both cancellous and cortical bones. Additionally, it exerted beneficial effects on both femurs and vertebrae in ovariectomized (OVX) mice. Mechanistic studies showed that AVL-95% inhibited osteoclastogenesis by suppressing RANKL signaling. Importantly, AVL-95% did not exhibit apparent toxicity in acute and chronic toxicity evaluations. Collectively, our work reveals a previously unknown efficacy of AVL in PMO intervention and an underlying mechanism of this efficacy, highlighting the anti-PMO application potential of AVL.

1. Introduction

Osteoporosis is characterized by bone loss and micro-architectural deterioration of bone tissue, primarily attributed to disrupted bone remodeling. Bone remodeling results from the coordinated actions of osteoblasts and osteoclasts, with the latter mediating old bone resorption and the former promoting new bone formation [1]. The functional balance between osteoblasts and osteoclasts maintains the dynamic equilibrium of bone mass and structure, whereas an imbalance frequently leads to osteoporosis [2]. Postmenopausal osteoporosis (PMO), resulting from estrogen deficiency due to ovarian failure, represents the most common type of osteoporosis. PMO causes bone fragility, deformation, and fractures, which seriously affect the physical health and quality of life of postmenopausal women [3, 4]. Estrogen deficiency frequently increases the generation and activity of osteoclasts, leading to an osteoclast–osteoblast imbalance followed by bone loss and architectural damage [5].

Osteoclasts are multinucleated giant cells mainly distributed on the bone surface and around intraosseous blood vessel channels. They originate from either circulating blood monocytes or bone marrow-resident precursors [6]. The receptor activator of nuclear factor-kappa B ligand (RANKL) signaling pathway is essential for inducing osteoclast generation from progenitor cells and for maintaining osteoclast survival and function. In this signaling pathway, RANKL binds to its cognate receptor RANK on the plasma membrane to initiate a downstream signaling cascade [7, 8]. Cytoplasmic transduction of RANKL signaling is mediated by several factors, including mitogen-activated protein kinases (MAPKs), nuclear factor-kappa B (NF-κB), and protein kinase B (PKB) [9, 10].

Given that osteoclast hyperactivation is a major pathological mechanism in PMO, targeting osteoclasts to reduce their generation and activity represents an important therapeutic approach. Therefore, clinical drugs for treating PMO are mainly osteoclast inhibitors, including calcitonin, bisphosphonates, hormone replacement therapy (HRT), and RANKL monoclonal antibodies [11, 12]. Hormone replacement therapy (HRT) is the traditional "gold standard" treatment for PMO [13], effectively preventing bone loss and reducing fracture incidence. However, long-term use of HRT, especially without concomitant progesterone, frequently causes estrogen-related side effects, primarily manifested as an increased risk of breast and endometrial cancers [14].

Apocynum venetum leaf (AVL) is a traditional Chinese medicine (TCM) that is also used as a vegetable in Nigeria [15]. It has been developed and produced as health foods such as tea, beverages, chocolate, and chewing gum. Previous studies have shown that AVL possesses various pharmacological activities, including blood pressure reduction, anti-oxidation, anti-depression, anti-anxiety, and cholesterol-lowering effects [15-17]. In this study, we re-

* Corresponding author.
E-mail addresses: linting@xmu.edu.cn (T. Lin); huzhou@xmu.edu.cn (H. Zhou)
Δ These authors contributed equally to this work.

https://doi.org/10.1016/S1875-5364(26)61186-7
Copyright © 2026, China Pharmaceutical University. Published by Elsevier B.V. All rights are reserved.

ported for the first time the anti-PMO activity of AVL extract. Moreover, we defined the effective fractions of AVL extract. Mechanistically, we revealed that AVL extract inhibits RANKL signaling to suppress osteoclastogenesis.

2. Materials and methods

2.1. Materials

Apocynum venetum leaf (AVL) was purchased from Guangdong HuiQun Chinese Traditional Medicine Co., Ltd. TRAP staining kit was purchased from Cosmo Biology (PMC-AK40F-COS). RANKL (ab2700070), M-CSF (ab259396), and JNK and p-JNK antibodies were purchased from Abcam. p65, p-p65, ERK and p-ERK antibodies were purchased from Santa Cruz Biotechnology. p38 and p-p38 antibodies were purchased from Invitrogen.

2.2. Preparation of AVL extract and its fractions

Dried AVL (20 kg) was immersed in 60% ethanol (*V/V*, 270 L) for 12 h and then heated under reflux four times (1 h each). The extracted solutions were combined and filtered, and then concentrated using a vacuum evaporator to obtain the AVL extract. The AVL extract (about 2.5 kg) was separated using microporous resin (D101) with a gradient of EtOH-H_2O (0 : 100; 25 : 75; 50 : 50; 75 : 25; 95 : 5, *V/V*, 100 L for each step) as elution buffer to obtain five fractions. The eluted fractions were designated as AVL-W (elution with water, 345.57 g), AVL-25% (elution with 25% ethanol, 780.87 g), AVL-50% (elution with 50% ethanol, 412.88 g), AVL-75% (elution with 75% ethanol, 59.25 g), and AVL-95% (elution with 95% ethanol, 48.83 g). The weight proportions of the five fractions in the total extract were 14.31%, 32.34%, 17.10%, 2.45%, and 2.02%, respectively.

2.3. Cell culture

RAW264.7 cells were cultured at 37 °C in a humid atmosphere containing 5% CO_2 in DMEM supplemented with 10% FBS, and were seeded at a density of 1×10^5 cells/cm^2. Bone marrow-derived monocytes (BMMs) were isolated from C57BL/6 mice aged 6–8 weeks. The mice were sacrificed under anesthesia and immersed in 70% ethanol for 5 min, and the femurs and tibias were harvested. Whole bone marrow cells were flushed from the femurs and tibias, seeded in a 10-cm dish, and cultured in α-MEM supplemented with 10% FBS at a density of 5×10^4 cells/cm^2. Cells were maintained by macrophage colony-stimulating factor (M-CSF, 50 ng·mL^{-1}).

2.4. In vitro osteoclast induction and TRAP staining

BMMs cultured in a 96-well plate at a density of 5×10^4 cells/cm^2 were incubated with M-CSF (50 ng·mL^{-1}), RANKL (50 ng·mL^{-1}) and/or AVL-95% fraction. Osteoclasts with more than 3 nuclei were produced after induction of M-CSF and RANKL for 3–4 days. Mature osteoclasts with larger volume and more nuclei were observed after 7 days of induction. Cells were fixed with 4% paraformaldehyde for 10 min at room temperature and stained using a TRAP staining kit (Cosmo Bio, PMC-AK40F-COS) at 37 °C for 1 h. The stained cells were observed under an upright microscope and photographed.

2.5. Bone resorption pit assay

BMMs were seeded on 96-well Corning Osteo Assay plates (Corning, Tewksbury, MA, USA), and stimulated with M-CSF (50 ng·mL^{-1}), RANKL (50 ng·mL^{-1}) and/or AVL-95% fraction. After 7 days, cells on the plates were removed using 5% sodium hypochlorite solution. Light microscopic images were captured for each well, and pit areas were quantified using ImageJ software.

2.6. Quantitative real-time PCR (RT-PCR)

BMMs seeded in a 6-well plate at a density of 5×10^4 cells/cm^2 were stimulated by M-CSF (50 ng·mL^{-1}), RANKL (50 ng·mL^{-1}) and/or AVL-95% fraction for 36 h and 72 h. Total RNA was isolated using TRIzol™ Reagent (Thermo Fisher Scientific) and then reverse-transcribed into cDNA by using a Hifair™ II 1st Strand cDNA Synthesis SuperMix Kit according to the manufacturer's instructions. SYBR Green was used to quantify the PCR products of the specific genes with *Gapdh* gene as an internal control. The relative mRNA levels of the specific genes were normalized to *Gapdh* and calculated by using the $2^{-\Delta\Delta Ct}$ method. PCR primers used were as follows: *Gapdh* (forward, 5′-ATCAAGAAGGTGGTGAAGCA-3′ and reverse, 5′-GTCGCTGTTGAAGTCAGAGGA-3′). *Nfatc1* (forward, 5′-CCCGTCACATTCTGGTCCAT-3′, and reverse, 5′-CAAGTAACCGTGTAGCTCCACAA-3′), *Trap* (forward, 5′-ACCAGCAAGGATTGCGAGGCAT-3′, and reverse, 5′-GGATGACAG ACGGTATCAGTGG-3′, *Calcr* (forward, 5′-CTGAAGCTTGAGCGCCTGAGTC-3′, and reverse, 5′-TGGGGTTGGGTGATTTAGAAGAAG-3′); *Ctsk* (forward, 5′-AAGATATTGGTGGCTTTGG-3′, and reverse, 5′-ATCGCTGCGTCCCTCT-3′).

2.7. MCF-7 cell viability assay

MCF-7 cells were seeded at 5×10^3 cells/well in a 96-well plate. After treatment with estradiol (E_2) and AVL-95% for 48 h, MTT (5 mg·mL^{-1}, dissolved in PBS) was added to each well and incubated at 37 °C for 48 h. The supernatant was discarded, and DMSO (100 μL) was added to dissolve the formazan crystals. Absorbance was measured at OD560 nm. Cell viability was calculated using the formula: Cell viability (%) = $[(OD_{experiment} - OD_{blank}) / (OD_{control} - OD_{blank})] \times 100\%$.

2.8. Western blotting

RAW264.7 cells seeded in a 6-well plate at a density of 1×10^5 cells/cm^2 were pretreated with E_2 or AVL-95% fraction for 1 h, followed by treatment with RANKL (50 ng·mL^{-1}) for 10 min. Cells were collected and lysed with lysis buffer (Beyotime Biotechnology, China) containing protease and phosphatase inhibitor cocktail. Protein samples were subjected to 10% SDS-PAGE and then transferred to a polyvinylidene difluoride membrane. The membranes were sequentially incubated with 5% skim milk, primary antibodies, and horseradish peroxidase (HRP)-conjugated secondary antibodies. Protein bands were visualized by exposure to X-ray film, and band densities were quantified using ImageJ software.

2.9. Ovariectomized rat and mouse models

The animal experimental protocols used in this study were approved by the Xiamen University Animal Center Committee (No. XMULAC20200205 and XMULAC20200015). Female Sprague–Dawley rats (3 months old), female C57BL/6 mice (10 weeks old) and Kunming mice (6 weeks old) were purchased from Shanghai SLAC Company and maintained under a standard housing condition (temperature, 22 °C; humidity, 40%–60%; light, 12 h of light/dark cycle; and pathogen-free-controlled environment). Before surgery, animals were anesthetized with 10% chloral hydrate (0.3 mL per 100 g for rats and 0.1 mL per 10 g for mice). Both ovaries were exposed through the incision and removed. The wound was closed in layers to prevent infection. Sham operations were performed using the same procedure but without ovary removal. One month after surgery, ovariectomized

animals were randomly divided into different groups. The vehicle used was 0.5% sodium carboxymethyl cellulose solution, and E_2 and AVL extract were dissolved in the vehicle for oral gavage.

2.10. Micro computed tomography (micro-CT) of bone

The middle to lower 1/3 of the left femurs (telecentric end) was examined by a Siemens Inveon PET/CT instrument. Bone mineral density (BMD) was calculated based on X-ray computed tomography, expressed in Hounsfield units (HU). The detection conditions for rat femurs were as follows: voltage, 80 kV; current, 500 μA; filter, 0.5 mm; exposure, 1000 ms; image width, 74.6; height, 49.7 (medium-low); total rotation, full; settle time, 1000 ms; estimated scan time, 792 s. Image and bone density analyses were performed using the image analysis software of this instrument.

The bones were also examined by a Bruker Skyscan1272 system. The instrument detection conditions for rat femurs were as follows: Source Voltage: 80 kV; Source Current: 125 μA; Image Pixel Size: 25 μm; Filter: Al 1 mm; Number of Files: 315; Number of Rows: 672; Number of Columns: 1008; Scan duration: 0h:8m:30s. The instrument detection conditions for mouse femurs and vertebrae are as follows: Source Voltage: 70 kV; Source Current: 142 μA; Image Pixel Size: 6 μm; Filter: Al 0.5 mm; Number of Files: 471; Number of Rows: 896; Number of Columns: 1344; Scan duration: 0h:16m:36s. Bone parameters were calculated with scanner software according to standardized protocols.

2.11. Tissue sections and TRAP staining

The femurs were fixed with 4% paraformaldehyde at 4 °C for 48 h, and then decalcified with 10% EDTA for 30 days. The distal end of the femurs was taken out for paraffin embedding and sectioning. The fifth lumbar vertebra (L5) of the mice were fixed in 4% paraformaldehyde at 4 °C for 24 h, and the undecalcified bones were embedded in methyl methacrylate. Plastic embedding (RM2255, Leica Microsystems, Wetzlar, Germany) and sectioning using the Leica TC65 microtome blade (14021626379, Leica Microsystems) were conducted as previously reported [18]. Histomorphometric analyses were carried out using the Osteomeasure Analysis System (OsteoMetrics, Atlanta, USA), and the standard procedures were used according to the procedure instruction [19].

2.12. Hematoxylin and eosin staining

The uteruses, livers, and kidneys were fixed with 4% paraformaldehyde at 4 °C for 48 h. After dehydration, the tissues were embedded in paraffin, sectioned, and stained with hematoxylin and eosin. The stained tissues were observed under a vertical microscope and photographed. The photographs were statistically analyzed, and femoral pathological parameters were obtained using a pathological image analysis software as previously described [20].

2.13. Acute and chronic toxicity evaluation

Kunming mice aged 6 weeks were randomly divided into groups of 7 mice each. Body weights were approximately 50 g for males and 40 g for females. The acute toxicity experiment employed the high-dose bolus administration method. Each mouse in the treatment group received AVL-95% fraction at a dose of 5 $g \cdot kg^{-1}$, and the control group was given the same volume of vehicle (0.5% CMC-Na), followed by the observation of body weight, respiratory performance, heart rate, appearance, behavior, secretions, urine and feces excretion for 14 days. Chronic toxicity evaluation was performed using female C57BL/6 mice. Mice were administrated with AVL-95% at 50 $mg \cdot kg^{-1} \cdot d^{-1}$ for 7 weeks, and mouse serum and uteruses were collected for examination.

2.14. Statistical analysis

Statistical analysis was performed using One-way ANOVA to determine the significance of the difference between the means of multiple groups. Values of $P < 0.05$ were considered statistically significant. The GraphPad Prism 6 (v6.0a; GraphPad, La Jolla, CA, USA) software was used for performing the calculations and statistical analysis.

3. Results

3.1. AVL extract inhibits the progression of osteoporosis in a rat OVX model

During the exploration of potential effects of AVL, we unexpectedly found that AVL extract inhibited osteoporosis in a rat ovariectomized (OVX) model. The rat OVX model is one of the mandatory items for pre-clinical research on osteoporosis drugs approved by the National Medical Products Administration (NMPA) [21, 22]. As shown in Fig.1A, compared with the sham group, the cancellous BMD of the femurs in the OVX group was dramatically reduced by approximately 50%. Histopathological examination revealed that the trabecular structure of the distal femurs was severely impaired in OVX rats (Fig. 1B). The values of trabecular bone area (Tb.Ar), trabecular thickness (Tb.Th), and trabecular number (Tb.N) were markedly reduced, whereas the trabecular separation (Tb.Sp) value was increased in OVX rats compared with sham rats (Fig. 1B). These results indicated the successful construction of the OVX-induced osteoporosis rat model.

Consistent with previous reports [23, 24], oral administration of estradiol (E_2) at 1 $mg \cdot kg^{-1} \cdot d^{-1}$ significantly increased the values of BMD, Tb.Ar, Tb.Th, and Tb.N, and reduced the Tb.Sp value in the OVX rats (Figs. 1A and 1B). AVL total extract was obtained by extraction of AVL with 60% ethanol (Fig. 2A), and oral administration of AVL extract to the OVX rats at 500 $mg \cdot kg^{-1} \cdot day^{-1}$ for 3 months was carried out [25, 26]. We found that AVL extract exhibited an effect similar to that of E_2 in ameliorating osteoporosis in the OVX rats (Figs. 1A and 1B). Thus, AVL extract has a potent anti-PMO effect in the OVX rats.

3.2. AVL-95% fraction inhibits the progression of osteoporosis in OVX rats

To identify the effective fractions of AVL extract, we separated AVL extract into several fractions by using macroporous resin adsorption chromatography. Through ethanol gradient elution, the total extract of AVL was separated into five fractions — AVL-W (elution with water), AVL-25% (elution with 25% ethanol), AVL-50% (elution with 50% ethanol), AVL-75% (elution with 75% ethanol), and AVL-95% (elution with 95% ethanol) (Fig. 2A), which accounted for 14.31%, 32.34%, 17.10%, 2.45%, and 2.02% of the total extract, respectively (Fig. 2B). We then evaluated the fractions by using the rat OVX model, and the rat-treating dosages of the fractions were calculated according to their proportions in the total extract. We found that AVL-50%, AVL-75%, and AVL-95% fractions exhibited strong effects on increasing cancellous BMD of the distal femurs in OVX rats, whereas the AVL-W fraction had no effect and AVL-25% fraction showed a weak effect (Fig. 2C). These results indicate that the active substances in AVL are not of high polarity.

Among the effective fractions, the treating dose of AVL-95% was the smallest, suggesting that the effective substances are highly concentrated in this fraction. We further confirmed that

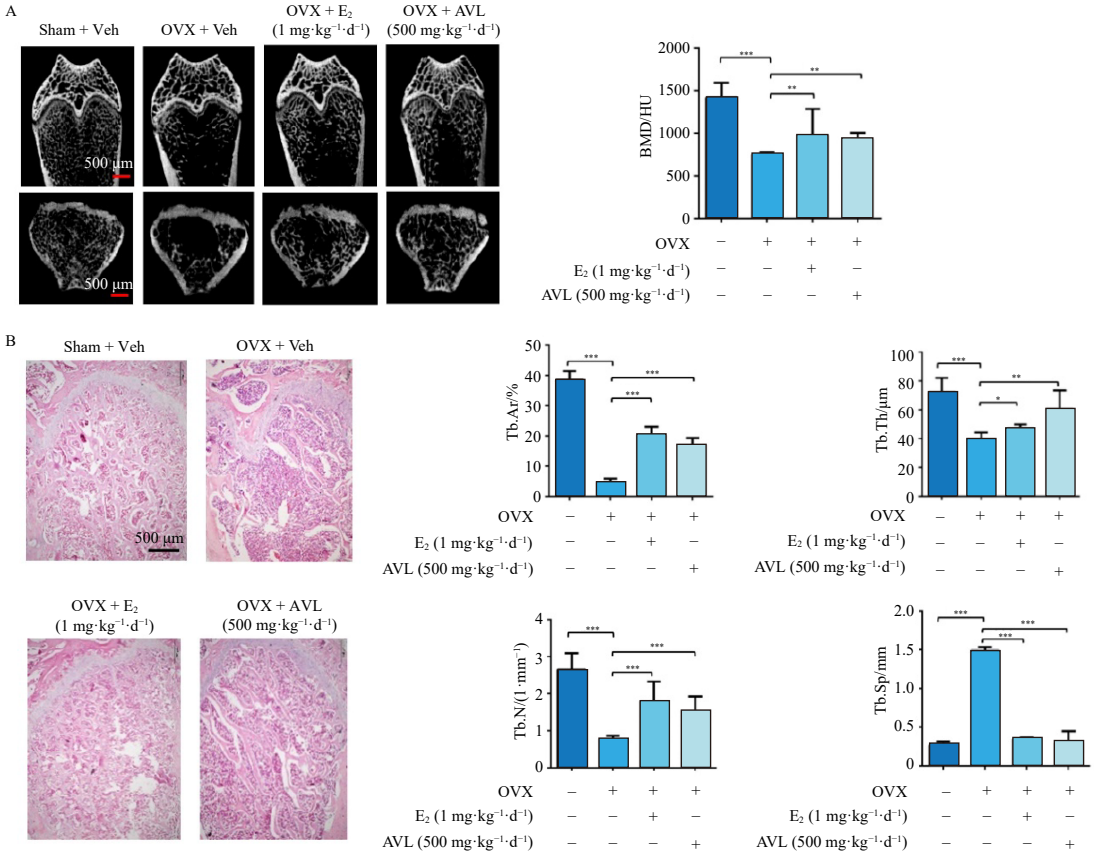

Fig. 1 AVL extract improves osteoporosis in OVX rats. Female Sprague–Dawley rats were subjected to bilateral ovariectomized (OVX) or sham (sham) operation, followed by the administration with vehicle (Veh), estradiol (E_2, 1 mg·kg^{-1}·d^{-1}) or *Apocynum venetum* leaf (AVL) extract (500 mg·kg^{-1}·d^{-1}) by oral gavage. After 3 months, rats were sacrificed and their femurs were collected. Bone mineral density was examined by micro computed tomography (micro-CT, Siemens), and two-dimensional structure of the longitudinal and transverse sections of the distal femurs was shown (A), scale bar = 0.5 mm. Hematoxylin and eosin staining was performed to examine the trabecular structure of the distal femurs, and the parameters of the bone trabecula were analyzed by the bone analysis software in strict accordance with bone tissue morphometry [39] (B), scale bar= 0.5 mm. BMD, bone mineral density; HU, Hounsfield unit; Tb.Ar, trabecular bone area; Tb.Th, trabecular thickness; Tb.N, trabecular number; Tb.Sp, trabecular separation. Data are expressed as mean ± SD, n = 3 in each group. $^{*}P < 0.05$; $^{**}P < 0.01$; $^{***}P < 0.001$. (One-way ANOVA).

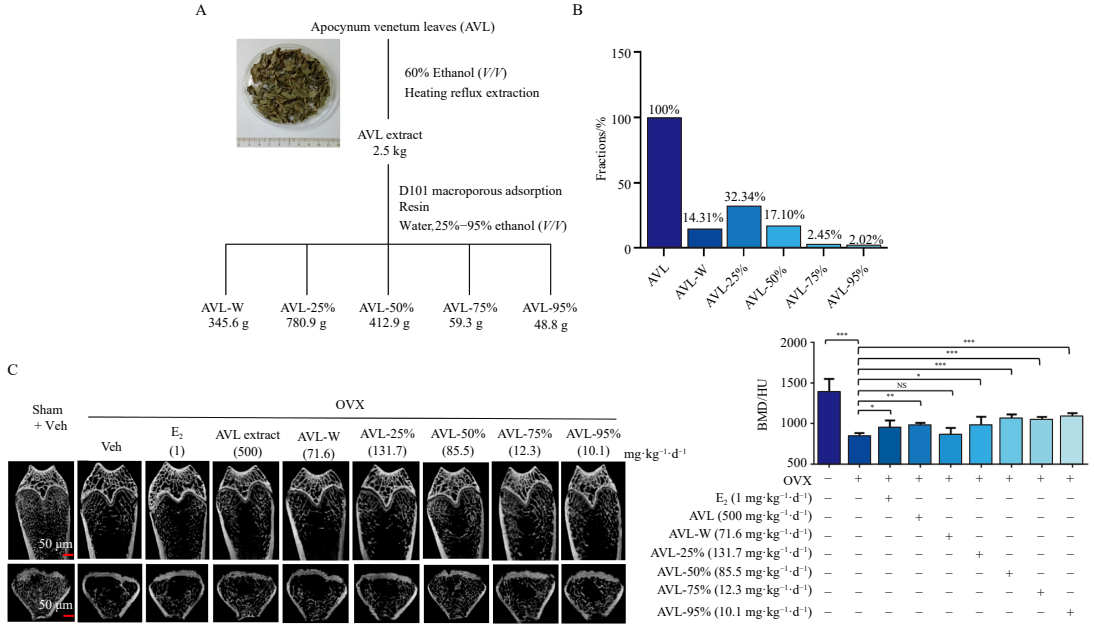

Fig. 2 AVL extract and its AVL-95% fraction improve osteoporosis in OVX rats. (A) The morphology of *Apocynum venetum* leaf (AVL) before extraction and the schematic diagram of the procedure of AVL extraction and extract separation. (B) The proportion of each fraction in the total extract of AVL. (C) Female Sprague–Dawley rats were subjected to bilateral ovariectomized (OVX) or sham operation (Sham) and then administered intragastrically with vehicle (Veh), E_2 (1 mg·kg^{-1}·d^{-1}), AVL extract (500 mg·kg^{-1}·d^{-1}), or the different fractions of AVL extract at the indicated doses. After 3 months, rats were sacrificed and their femurs were collected. Bone morphometry was examined by micro-CT (Siemens, PET-CT), and two-dimensional structure of the longitudinal and transverse sections of the distal femur was shown (left panel). Bone mineral density of the cancellous was quantified and statistically analyzed (right panel). scale bar = 0.5 mm. BMD, bone mineral density; HU, Hounsfield unit. Data are expressed as mean ± SD, n = 3 in each group. NS, non-significant; $^{*}P < 0.05$; $^{**}P < 0.01$; $^{***}P < 0.001$. (One-way ANOVA).

oral administration of AVL-95% at the doses of 10 and 50 mg·kg^{-1}·d^{-1} significantly increased the values of BMD, bone volume fraction (BV/TV), and Tb.N, and reduced the values of Tb.Sp of the femoral cancellous bones in the OVX rats (Fig. 3). In addition, the efficacy of AVL-95% fraction was comparable to that of E_2 at 1 mg·kg^{-1}·d^{-1}(Fig. 3).

3.3. AVL-95% fraction inhibits the progression of osteoporosis in a mouse OVX model

We further investigated whether the AVL-95% fraction exhibited cross-species efficacy against PMO using a mouse OVX model. Compared with sham mice, the microstructure of the femoral cancellous bones was impaired and bone density was decreased in OVX mice (Fig. 4). The total flavonoids of *Rhizoma Drynariae* (TFRD), the main component of Qianggu Capsule, a patented TCM, have been widely used in treating PMO. Consistently, we found that TFRD at 200 mg·kg^{-1}·d^{-1} ameliorated the cancellous microstructure in OVX mice (Fig. 4). As expected, administration of AVL-95% at both 50 and 200 mg·kg^{-1}·d^{-1} showed potent efficacy in inhibiting the deleterious progression of the femoral cancellous bones in the OVX mice (Fig. 4). Statistical analysis showed that AVL-95% at 200 mg·kg^{-1}·d^{-1} significantly increased BMD, BV/TV, Tb.N and Tb.Th, and decreased Tb.Sp and the structure model index (SMI) of femoral cancellous bones in OVX mice (Fig. 4). It was noteworthy that AVL-95% at 200 mg·kg^{-1}·d^{-1} showed similar or better effect than TFRD on inhibiting osteoporosis.

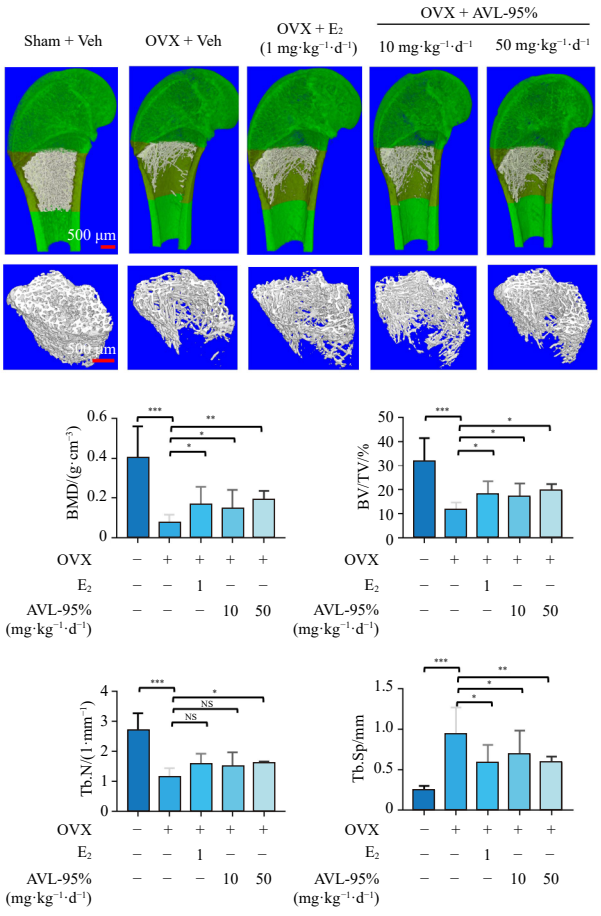

Fig. 3 AVL-95% fraction improves osteoporosis in OVX rats. The OVX rats were administered intragastrically with E_2 (1 mg·kg^{-1}·d^{-1}) and AVL-95% (10 and 50 mg·kg^{-1}·d^{-1}) for 3 months, and the cancellous bones of femurs were examined by micro-CT (Bruker，Skyscan1272). The three-dimensional (3D) reconstruction of the cancellous bones of the distal femur in the region of interest was shown. Scale bars = 0.5 mm. BMD, bone mineral density; BV/TV, bone volume fraction; Tb.N, trabecular number; Tb.Sp, trabecular separation. Data are expressed as mean ± SD, n = 5 in each group. NS, non-significant; $^{*}P < 0.05$; $^{**}P < 0.01$; $^{***}P < 0.001$. (One-way ANOVA).

Interestingly, AVL-95% also exhibited potent effect on strengthening the femoral cortical bone in the OVX mice. As shown in Fig. 5A, both AVL-95% and E_2 increased the cortical BMD (CBMD), cortical bone fraction (Ct.Ar/Tt.Ar, cortical bone area/total cross-sectional area), and cortical thickness (Ct.Th) of the femurs while reducing the marrow area (Ma.Ar) of the femurs in OVX mice. Ovariectomy also caused damage to the vertebral structure, as indicated by decreased BMD, BV/TV, and Tb.Th of the vertebrae in OVX mice (Fig. 5B). Both E_2 and AVL-95% increased these vertebral indexes in OVX mice. Thus, the beneficial effect of AVL-95% is not only to femurs but also to vertebrae in OVX mice.

3.4. AVL-95% inhibits osteoclast formation and function

A major mechanistic cause of PMO is the functional imbalance between osteoclasts and osteoblasts, most often resulting from excessive osteoclast generation or activation. Thus, inhibiting osteoclast generation or activation is a well-established and effective approach for treating osteoporosis [27-29]. To gain mechanistic insights into the effects of AVL-95%, we investigated whether AVL-95% regulated osteoclast formation and function. Tartrate-resistant acid phosphatase (TRAP) is a marker enzyme of osteoclasts, and TRAP-positive osteoclasts can be stained red with staining reagent in the presence of sodium tartrate. We found that osteoclast hyperplasia occurred in the lumbar vertebrae of OVX mice, as evidenced by increased TRAP staining and elevated osteoclast number per bone perimeter (N.Oc/B.Pm) and osteoclast surface per bone surface (Oc.S/BS) indexes (Fig. 6A). Administration of AVL-95% effectively reduced TRAP staining as well as the values of N.Oc/B.Pm and Oc.S/BS.

We further isolated BMMs from mice administered vehicle or AVL-95% and evaluated the osteoclastogenic potency of the primary BMMs *in vitro*. Treatment with M-CSF and RANKL significantly induced osteoclast formation — large multinucleated cells — from primary BMMs isolated from vehicle-treated OVX mice but not from sham mice (Fig. 6B). This result indicates that BMMs from OVX mice possess much stronger osteoclastogenic potency than those from sham mice, most likely due to ovariectomy-induced estrogen deficiency. However, the osteoclastogenic potency of BMMs isolated from AVL-95%-treated OVX mice was substantially diminished compared with that of BMMs from vehicle-treated OVX mice (Fig. 6B). Thus, AVL-95% reduces the osteoclastogenesis potency in vivo.

The inhibitory effect of AVL-95% on osteoclastogenesis was further validated by our *in vitro* results. BMMs purified from the mice without any treatment were cultured *in vitro* and then treated with M-CSF and RANKL together with vehicle, E_2 or AVL-95%. Treatment with the combination of M-CSF and RANKL, but not M-CSF alone, significantly induced the emergence of osteoclasts (Fig. 7A). Thus, RANKL is essential for osteoclastogenesis. As expected, both AVL-95% at 5 μg·mL^{-1} and E_2 at 100 nmol·L^{-1} strongly inhibited RANKL-induced osteoclast formation with a comparable efficacy. In addition, AVL-95% showed a dose-dependent inhibitory effect on osteoclast formation (Fig. S1). After 7 days of induction by M-CSF and RANKL, osteoclasts became mature and functional, exhibiting bone resorption capability as indicated by the wide areas of absorption pits on the Corning Osteo Assay plates (Fig. 7B). Both AVL-95% and E_2 dramatically reduced the resorption area (Fig. 7B). Thus, the formation and/or the activity of osteoclasts is inhibited by AVL-95%.

3.5. AVL-95% inhibits RANKL signaling

We further explored the mechanisms underlying AVL-95%

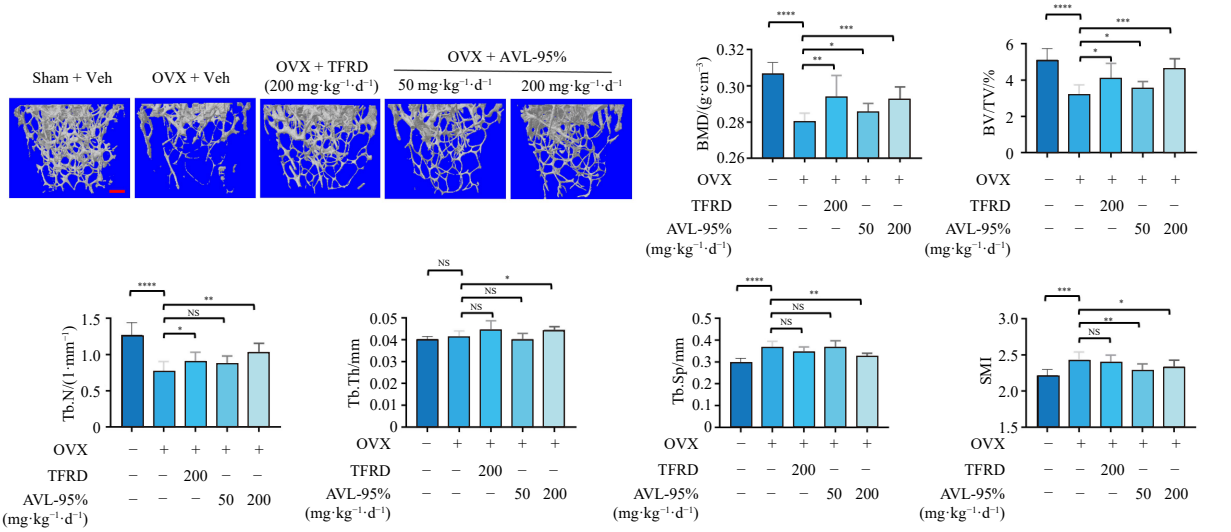

Fig. 4 AVL-95% increases bone mineral density and improves bone tissue microstructure in OVX mice. Female C57BL/6 mice were subjected to bilateral OVX or sham operation. One month after surgery, mice were administered intragastrically with vehicle (Veh), TFRD (200 mg·kg^{-1}·d^{-1}) or AVL-95% (50 and 200 mg·kg^{-1}·d^{-1}). After 10 weeks, mice were sacrificed, and their femurs were collected and examined by micro-CT (Bruker, Skyscan1272). The cancellous bone of femurs was analyzed by micro-CT, and the 3D reconstructions of the trabecular bone were obtained using the software Skyscan-1272. Scale bar = 0.5 mm. TFRD, total flavonoids of *Rhizoma Drynariae*; BMD, bone mineral density; BV/TV, bone volume fraction; Tb.N, trabecular number; Tb.Th, trabecular thickness; Tb.Sp, trabecular separation; SMI, structure model index. Data are expressed as mean ± SD, n = 5 in each group. NS, non-significant; $^{*}P < 0.05$; $^{**}P < 0.01$; $^{***}P < 0.001$; $^{****}P < 0.0001$. (One-way ANOVA).

action in osteoclastogenesis. We found that RANKL-induced expression of osteoclast marker genes — *Nfatc1*, *Trap*, *Calcr* and *Ctsk* — in BMMs was potently inhibited by AVL-95% (Fig. 8A), confirming its inhibitory effect on osteoclastogenesis. The master

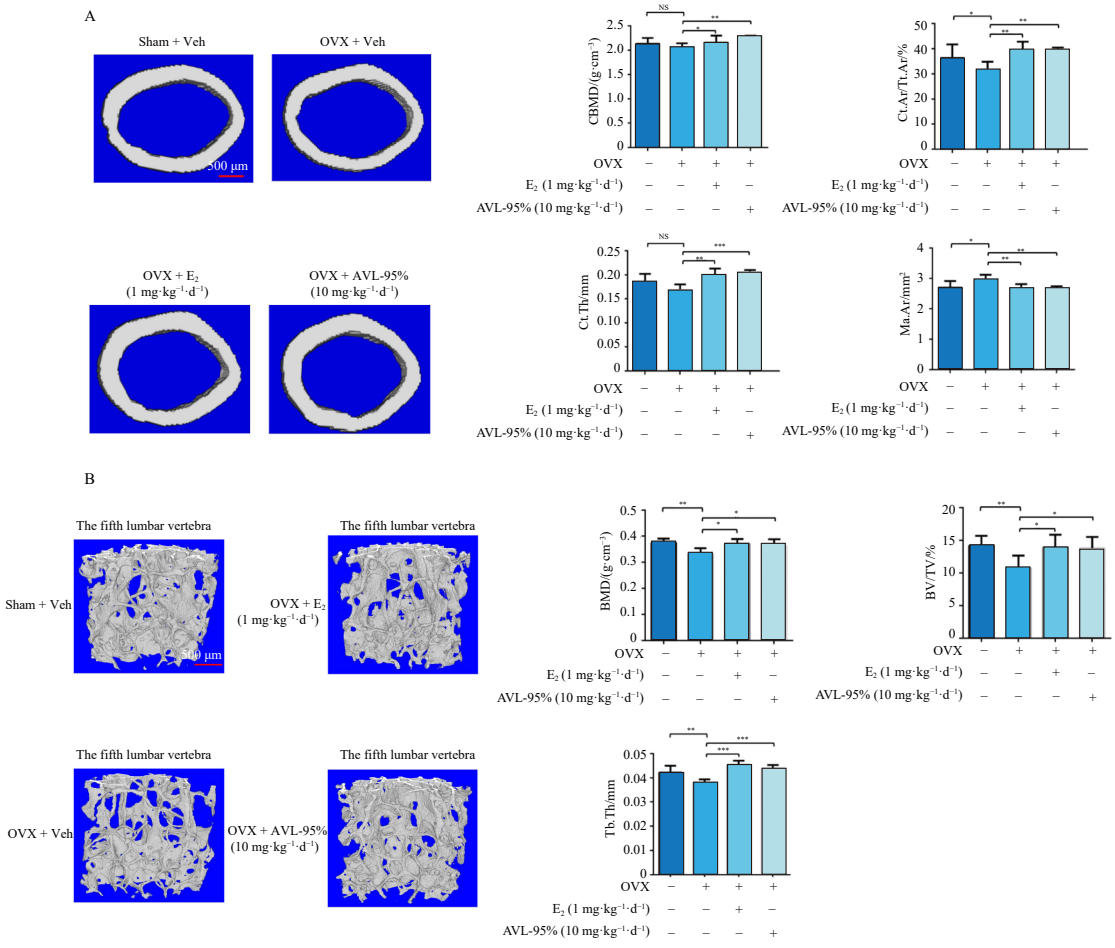

Fig. 5 AVL-95% exerts beneficial effect on cortical bone and lumbar vertebrae in OVX mice. Female C57BL/6 mice were subjected to bilateral OVX or sham surgery. One month after surgery, the mice were administered intragastrically with vehicle (Veh), E_2 (1 mg·kg^{-1}·d^{-1}) or AVL-95% (10 mg·kg^{-1}·d^{-1}). After 10 weeks, mice were sacrificed, and their femurs (A) and 5th lumbar vertebrae (B) were collected. The femoral cortical bones (A) and the 5th lumbar vertebrae (B) were analyzed by micro-CT (Bruker, Skyscan1272) and the 3D reconstructions were obtained using the software Skyscan-1272. Scale bars = 0.5 mm. BMD, bone mineral density; BV/TV, bone volume fraction; Tb.Th, trabecular thickness. CBMD, cortical BMD; Ct.Ar/Tt.Ar, cortical bone fraction (cortical bone area/total cross-sectional area); Ct.Th, cortical thickness; Ma.Ar, marrow area. Data are expressed as mean ± SD, n = 5 in each group. $^{*}P < 0.05$; $^{**}P < 0.01$; $^{***}P < 0.001$. (One-way ANOVA).

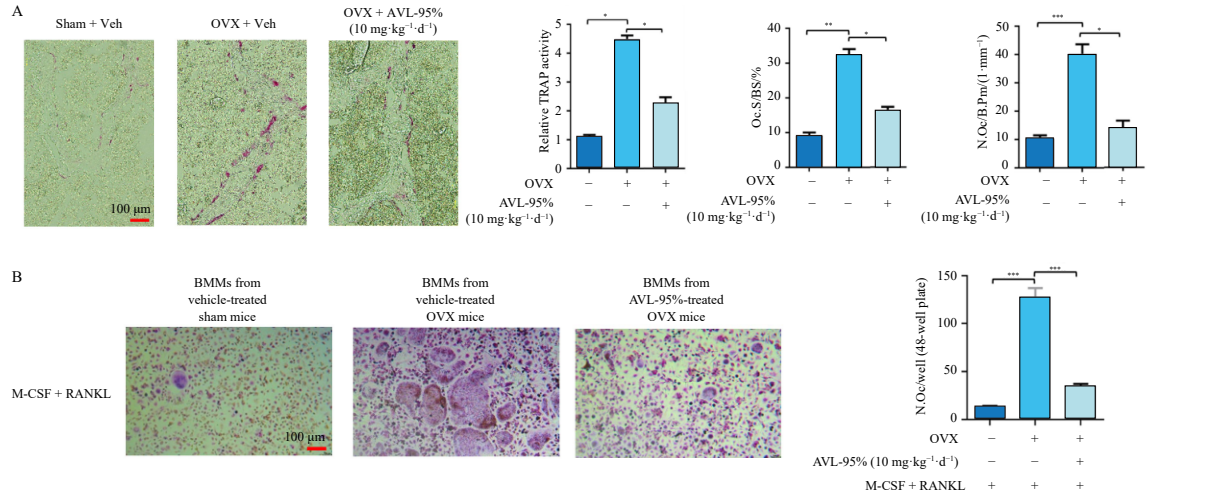

Fig. 6 AVL-95% fraction inhibits osteoclast formation *in vivo*. (A) After treatment with AVL-95% fraction (10 mg·kg^{-1}·d^{-1}) for 10 weeks, the right femurs of sham and OVX mice were taken out to make non-decalcified hard tissue slices, followed by TRAP staining. ImageJ software was used to analyze the activity of TRAP, and osteomeasure analysis system software (OsteoMetrics) was used to calculate osteoclast parameters. Scale bar = 200 μm. (B) The OVX mice were treated with AVL-95% fraction (50 mg·kg^{-1}·d^{-1}) for 8 weeks. BMMs purified from bone marrows of sham and OVX mice were stimulated with the inducer (50 ng·mL^{-1} RANKL and 50 ng·mL^{-1} M-CSF) for 3 days, followed by TRAP staining. The stained osteoclasts (the number of nuclei ≥ 3) were counted. Scale bar = 100 μm. N.Oc/B.Pm, osteoclast number per bone perimeter; Oc.S/BS, osteoclast surface per bone surface. Data are expressed as mean ± SD, n = 5 in each group. $^{*}P < 0.05$; $^{**}P < 0.01$; $^{***}P < 0.001$. (One-way ANOVA)

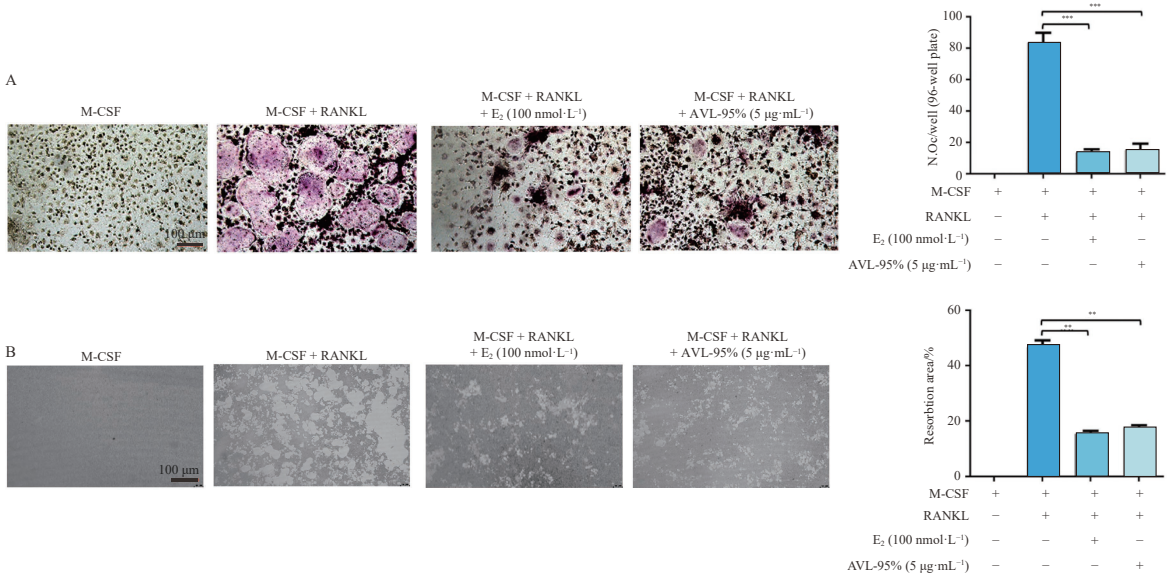

Fig. 7 AVL-95% fraction inhibits osteoclast formation *in vitro*. (A) BMMs purified from bone marrows of C57BL/6 mice were stimulated with RANKL (50 ng·mL^{-1}) and M-CSF (50 ng·mL^{-1}) together with E_2 (100 nmol·L^{-1}) or AVL-95% fraction (5 μg·mL^{-1}) for 7 days, followed by TRAP staining. TRAP-staining positive cells with three or more nuclei were counted. Scale bar = 100 μm. (B) BMMs seeded on 96-well Corning Osteo Assay plates were treated with M-CSF (50 ng·mL^{-1}) and RANKL (50 ng·mL^{-1}) together with E_2 (100 nmol·L^{-1}) or AVL-95% fraction (5 μg·mL^{-1}) for 7 days. Cells were removed by adding 5% sodium hypochlorite solution, and microscopic images were captured for each well. Pit areas were quantified by ImageJ software. Scale bar = 100 μm. Data are expressed as mean ± SD, n = 3 in each group. $^{**}P < 0.01$; $^{***}P < 0.001$. (One-way ANOVA).

transcription factor driving osteoclastic differentiation is nuclear factor of activated T cells 1 (NFATc1), which is encoded by the Nfatc1 gene and induced by the transcription factor AP-1, a heterodimer of c-Jun and c-Fos. AP-1 is regulated by MAPKs, including c-Jun N-terminal kinase (JNK), p38, and extracellular signal-regulated kinase (ERK), which are downstream transducers of RANKL signaling [9]. We then investigated whether AVL-95% inhibited RANKL-induced activation of these MAPKs. As shown in Fig. 8B, treatment of BMMs with RANKL strongly activated JNK, p38 and ERK, as indicated by their increased phosphorylation. Consistent with previous reports [30, 31], E_2 dose-dependently inhibited RANKL signaling in BMMs, which, to some extent, accounts for its inhibitory effect on osteoclastogenesis. Similarly, AVL-95% fraction also dose-dependently inhibited RANKL-induced phosphorylation of the MAPKs (Fig. 8B). Moreover, RANKL-induced phosphorylation of p65, a subunit of NF-κB that plays an important role in RANKL-induced osteoclastogenesis, was also inhibited by AVL-95% in BMMs (Fig. 8C). Thus, the AVL-95% fraction appears to inhibit RANKL signaling to impede osteoclast differentiation, thereby contributing to the suppression of osteoporosis.

3.6. AVL-95% has no apparent toxicity

To evaluate the drug property of AVL-95% fraction, its acute and chronic toxicity were assessed. After a single oral administration of AVL-95% fraction at 5 g·kg^{-1}, no abnormalities in respiratory performance, appearance, behavior, secretions, or urine and feces excretion were observed in mice. No significant changes in body weight or the weight indexes of the hearts, livers, spleens, lungs, and kidneys were observed in either male or female mice

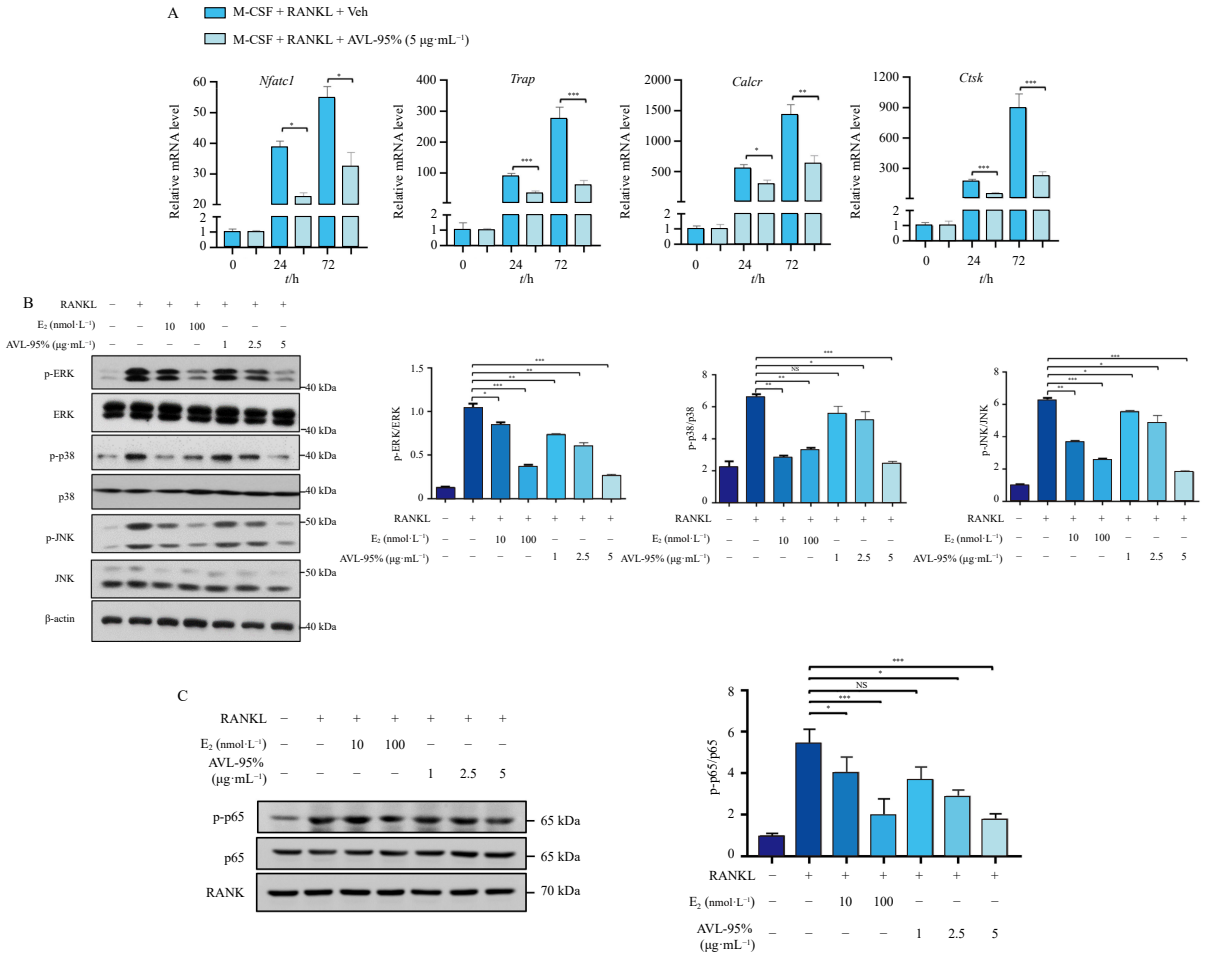

Fig. 8 AVL-95% fraction inhibits RANKL signaling. (A) BMMs purified from bone marrows of C57BL/6 mice were stimulated with RANKL (50 ng·mL^{-1}) and M-CSF (50 ng·mL^{-1}) together with vehicle (Veh) or AVL-95% fraction (5 μg·mL^{-1}) for 24 h or 72 h. The mRNA expression levers of *Nfatc1*, *Trap*, *Ctsk*, and *Calcr* were detected by quantitative real-time PCR. (B,C) RAW264.7 cells were pre-treated with E_2 or AVL-95% fraction for 1 h, and subsequently stimulated with RANKL (50 ng·mL^{-1}) for 10 min. Cell lysates were subjected to western blotting analysis of the phosphorylation of JNK, p38, ERK and p65, and the density of the protein bands was quantified by ImageJ software. Data are expressed as mean ± SD, n = 3 in each group. NS, non-significant; $^{*}P < 0.05$; $^{**}P < 0.01$; $^{***}P < 0.001$. (One-way ANOVA).

(Figs. S2A and S2B). Moreover, the mice treated with AVL-95% fraction were all survived. Chronic toxicity study showed that AVL-95% at the dosage of 50 mg·kg^{-1}·d^{-1} for 7 weeks did not affect the weight of mice (Fig. S2C). The blood biochemical indexes of mouse livers (aspartate aminotransferase (AST) and alanine aminotransferase (ALT)) and kidneys (urea and uric acid (UA)) were not affected by the administration of AVL-95% fraction (Fig. 9A). Tissue sections showed that AVL-95% treatment caused no apparent pathological changes in livers and kidneys (Fig. 9B). These results preliminarily indicate that AVL-95% fraction has a favorable safety profile in rodents.

A major adverse effect of HRT is the increased risk of endometrial hyperplasia due to its strong estrogenic effects. Natural extracts often contain estrogenic substances that exert beneficial effects on osteoporosis by acting similarly to estrogen. Estrogenic effects can be reflected in the maintenance of uterine morphometry and function. In our OVX rat and mouse models, significant endometrial shrinkage and uterine weight reduction were observed in both mice and rats (Fig. 9C and Fig. S3), resulting from the estrogen deficiency. Treatment with E_2 (1 mg·kg^{-1}) in mice and rats robustly rescued OVX-induced endometrial shrinkage and uterus weight loss (Fig. 9C and Fig. S3), exhibiting the strong potency of E_2 in uterine stimulation. However, AVL-95% fraction did not show apparent effects on endometrial thickness and uterus weight in the OVX mice and rats (Fig. 9C and Fig. S3). Moreover, E_2 potently promoted the viability of the breast cancer MCF-7 cells, whereas AVL-95% did not show an apparent effect (Fig. 9D). These results indicate that AVL-95% fraction does not possess estrogenic activity.

4. Discussion

Osteoporosis is a chronic but generally not a life-threatening disease, and patients need to take medicine for a long-term or even for their entire lives [32, 33]. Thus, in addition to satisfactory efficacy, extremely low toxicity should be the primary property of the anti-osteoporosis drugs, which is a quality generally lacking among current clinical osteoporosis medications. TCMs, especially those with homology of medicine and food, are characterized by low toxicity and are thereby suitable for long-term treatment [34, 35]. Here, we found that the extract of AVL, a TCM with both nutritional and medicinal values, had strong anti-osteoporosis activity.

Although AVL has been used both as food and medicine for a long history [36, 37], the data concerning its safety are still missing. In addition, the preparation of AVL extract and the AVL-95% fraction involves ethanol extraction, which differs from the traditional preparation of AVL for Chinese medicine that typically uses water as the solvent. Thus, assessing the toxicity of the AVL-95% fraction before further consideration of its application in osteoporosis is important. Our acute and chronic toxicity experiments showed no significant toxicity of the AVL-95% fraction in mice, supporting its safety and the feasibility of the preparation procedure. The clinical use of estrogen can effectively prevent and treat PMO, but estrogen use generally cannot exceed 2 years, primarily due to its estrogenic side effects [38]. Our study showed

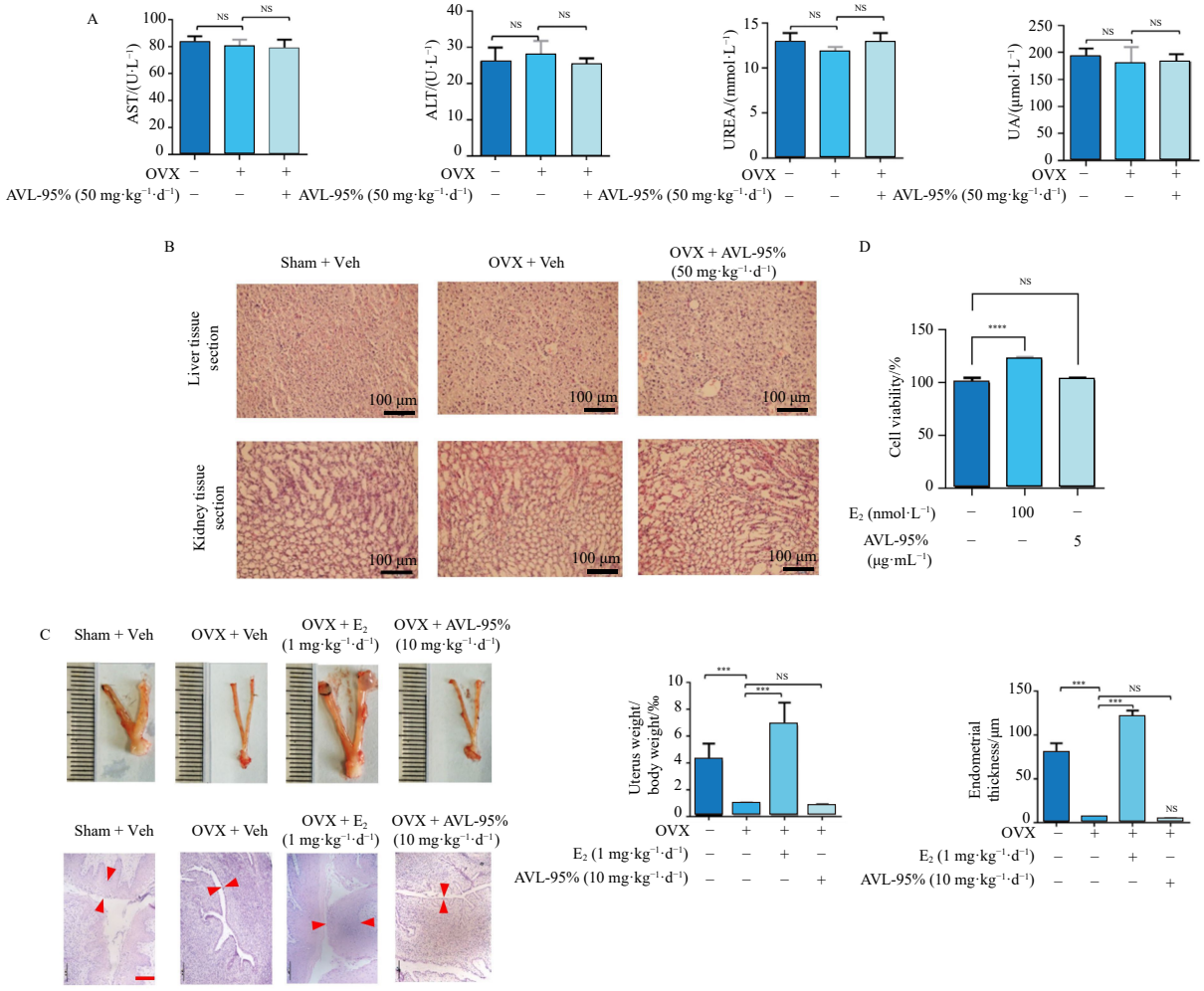

Fig. 9 AVL-95% fraction has no obvious toxicity. (A, B) The OVX C57BL/6 mice were administered intragastrically with AVL-95% fraction (50 mg·kg^{-1}·d^{-1}) for 7 weeks. Blood samples were drawn from orbit for quantification of AST, ALT, urea and uric acid (UA) (A). The morphometric examination of mouse livers and kidneys was performed by hematoxylin and eosin staining. Scale bar = 100 μm (B). (C) The OVX rats were administered intragastrically with E_2 (1 mg·kg^{-1}·d^{-1}) and AVL-95% fraction (10 mg·kg^{-1}·d^{-1}) for 10 weeks. The size of uterus and the thickness of endometrium were measured. The spacing between the two red arrowheads indicates the thickness of the endometria. Scale bar = 500 μm. (D) MCF-7 cells were treated with E_2 and AVL-95% for 48 h, and cell viability was measured by MTT assay. Data are expressed as mean ± SD, n = 5 in each group. NS, non-significant; $^{***}P < 0.001$; $^{****}P < 0.0001$. (One-way ANOVA).

that AVL-95% fraction had comparable effect as E_2 on ameliorating osteoporosis. However, it did not show any estrogenic side effects, representing a favorable factor that warrants its long-term usage for PMO treatment.

The AVL-95% fraction accounts for only about 2% of the total extract, yet it showed an effect comparable to that of the total extract. This indicates that the active ingredients can be effectively obtained by separation. Moreover, it is reasonable to presume that the AVL-95% fraction should be safer than the total extract, because approximately 98% of the ingredients, which may contain potentially toxic substances, were removed. Consistently, we did not detect significant toxicity of the AVL-95% fraction in our preliminary toxicity evaluation. However, the safety advantage of AVL-95% over the total extract should be confirmed by future systematic evaluation. The efficacy of AVL extract was demonstrated in both rat and mouse OVX models, indicating its cross-species efficacy. Moreover, AVL extract improved both cancellous and cortical bones. Additionally, it was beneficial to both femurs and vertebrae in OVX mice. These results indicate that the efficacy of AVL-95% in ameliorating osteoporosis may be systemic. The potent and systemic effect of AVL on PMO inhibition warrants further investigation.

Mechanistically, we found that AVL-95% inhibited the formation and function of osteoclasts, revealing one of the underlying mechanisms of its action. Moreover, AVL-95% was shown to inhibit RANKL signaling, through which AVL-95% likely exerts its osteoclastic inhibition. It has been reported that estrogen inhibits osteoclastogenesis by targeting and activating ERα to inhibit RANKL signaling. However, AVL-95% does not appear to act through ERα because it did not produce apparent estrogenic effects. Thus, how AVL-95% exerts its inhibitory effect on RANKL signaling requires further investigation.

Given the multiple mechanisms of PMO development and the complex ingredients in AVL extract, it is conceivable that AVL extract and the AVL-95% fraction exert anti-PMO effects through different substances working via different mechanisms, which may account for the systemic effect of the AVL-95% fraction. For example, the substances in the AVL-95% fraction might also regulate the formation and activity of osteoblasts to exert its anti-PMO efficacy.

To further explore the mechanisms of AVL-95% and the potential of its clinical application, it is necessary to determine which pure compounds in AVL-95% are responsible for the anti-osteoporosis effects in future studies. After identification of the active compounds, we will determine the therapeutic actions of these compounds, including inhibition of RANKL signaling. Finally, the targets of the active compounds and the molecular mechanisms of their actions will be elucidated.

5. Conclusions

In this work, we disclosed the previously unidentified effic-

acy of AVL extract in treating PMO and identified the effective fraction AVL-95%. Mechanistically, the AVL-95% fraction inhibits osteoclastogenesis by down-regulating RANKL signaling in the precursor cells of osteoclasts. Importantly, the AVL-95% fraction exhibits no apparent toxicity in rats and mice.

Funding

This work was supported by the National Natural Science Foundation of China (Nos. 32270758, 32070779 and 31770811).

Supporting information

Supporting information for this work can be obtained by contacting the corresponding authors *via* E-mail.

Declaration of competing interest

These authors have no conflict of interest to declare.

References

1 Yu H, Jiang L, Wan B, et al. The role of aryl hydrocarbon receptor in bone remodeling. *Prog Biophys Mol Biol*. 2018;134:44-49. https://doi.org/10.1016/j.pbiomolbio.2017.12.005.
2 Li Z, Li D, Chen R, et al. Cell death regulation: a new way for natural products to treat osteoporosis. *Pharmacol Res*. 2023;187:106635. https://doi.org/10.1016/j.phrs.2022.106635.
3 Lu L, Tian L. Postmenopausal osteoporosis coexisting with sarcopenia: the role and mechanisms of estrogen. *J Endocrinol*. 2023;259(1):e230116. https: // https://doi.org/10.1530/JOE-23-0116.
4 Lisco G, Triggiani D, Giagulli VA, et al. Endocrine, metabolic, and immune pathogenesis of postmenopausal osteoporosis: is there a therapeutic role in natural products? *Endocr Metab Immune Disord Drug Targets*. 2023;23(10):1278-1290. https://doi.org/10.2174/1871530323666230330121301
5 Jiang X, Kagan R. Hormone therapy for postmenopausal osteoporosis management. *Climacteric*. 2022;25(1):50-55. https://doi.org/10.1080/13697137.2021.1957818.
6 Novak S, Roeder E, Kalinowski J, et al. Osteoclasts derive predominantly from bone marrow-resident CX3CR1 + precursor cells in homeostasis, whereas circulating CX3CR1 + cells contribute to osteoclast development during fracture repair. *J Immunol*. 2020;204(4):868-878. https://doi.org/10.4049/jimmunol.1900665.
7 Lacey DL, Boyle WJ, Simonet WS, et al. Bench to bedside: elucidation of the OPG-RANK-RANKL pathway and the development of denosumab. *Nat Rev Drug Discov*. 2012;11(5):401-419. https://doi.org/10.1038/nrd3705.
8 Wang J, Ye T, Wang H, et al. The role of TAK1 in RANKL-induced osteoclastogenesis. *Calcif Tissue Int*. 2022;111(1):1-12. https://doi.org/10.1007/s00223-022-00967-z.
9 Lee K, Chung YH, Ahn H, et al. Selective regulation of MAPK signaling mediates RANKL-dependent osteoclast differentiation. *Int J Biol Sci*. 2016;12(2):235-245. https://doi.org/10.7150/ijbs.13814.
10 Xu Q, Chen G, Liu X, et al. Icariin inhibits RANKL-induced osteoclastogenesis *via* modulation of the NF-κB and MAPK signaling pathways. *Biochem Biophys Res Commun*. 2019;508(3):902-906. https://doi.org/10.1016/j.bbrc.2018.11.201.
11 Hiligsmann M, Evers SM, Ben Sedrine W, et al. A systematic review of cost-effectiveness analyses of drugs for postmenopausal osteoporosis. *Pharmacoeconomics*. 2015;33(3):205-224. https://doi.org/10.1007/s40273-014-0231-1.
12 Lewiecki EM. Emerging drugs for postmenopausal osteoporosis. *Expert Opin Emerg Drugs*. 2009;14(1):129-144. https://doi.org/10.1517/14728210902766813.
13 Cranney A, Wells GA. Hormone replacement therapy for postmenopausal osteoporosis. *Clin Geriatr Med*. 2003;19(2):361-370. https://doi.org/10.1016/S0749-0690(02)00078-2.
14 Gennari L, Rotatori S, Bianciardi S, et al. Treatment needs and current options for postmenopausal osteoporosis. *Expert Opin Pharmacother*. 2016;17(8):1141-1152. https://doi.org/10.1080/14656566.2016.1176147.
15 Xie W, Zhang X, Wang T, et al. Botany, traditional uses, phytochemistry and pharmacology of *Apocynum venetum* L. *(Luobuma): a review. J Ethnopharmacol*. 2012;141(1):1-8. https://doi.org/10.1016/j.jep.2012.02.003.
16 Wei JM. Progress in the study on the medical effects of *Apocynum venetum* (A. *lancifolium). J Tradit Chin Med*. 1988;8(1):34-36.
17 Xiang T, Wu L, Isah MB, et al. *Apocynum venetum*, a medicinal, economical and ecological plant: a review update. *Peer J*. 2023;11:e14966. https://doi.org/10.7717/peerj.14966
18 Fukuda T, Takeda S, Xu R, et al. Sema3A regulates bone-mass accrual through sensory innervations. *Nature*. 2013;497(7450):490-493. https://doi.org/10.1038/nature12115.
19 Sato S, Hanada R, Kimura A, et al. Central control of bone remodeling by neuromedin U. *Nat Med*. 2007;13(10):1234-1240. https://doi.org/10.1038/nm1640.
20 Xu R, Zhang C, Shin DY, et al. c-Jun N-terminal kinases (JNKs) are critical mediators of osteoblast activity *in vivo*. *J Bone Miner Res*. 2017;32(9):1811-1815. https://doi.10.1002/jbmr.3184
21 Tou JC. Resveratrol supplementation affects bone acquisition and osteoporosis: pre-clinical evidence toward translational diet therapy. *Biochim Biophys Acta Mol Basis Dis*. 2015;1852(6):1186-1194. https://doi.org/10.1016/j.bbadis.2014.10.003.
22 Mosekilde L. Assessing bone quality: animal models in preclinical osteoporosis research. *Bone*. 1995;17(4 Suppl):343S-352S.
23 Ma HR, Wang J, Qi HX, et al. Assessment of the estrogenic activities of chickpea (*Cicer arietinum* L.) sprout isoflavone extract in ovariectomized rats. *Acta Pharmacol Sin*. 2013;34(3):380-386. https://doi.org/10.1038/aps.2012.160.
24 Windahl SH, Andersson G, Gustafsson JA. Elucidation of estrogen receptor function in bone with the use of mouse models. *Trends Endocrinol Metab*. 2002;13(5):195-200. https://doi.org/10.1016/S1043-2760(02)00594-5.
25 Xiang J, Lan R, Tang YP, et al. *Apocynum venetum* leaf extract attenuates disruption of the blood-brain barrier and upregulation of matrix metalloproteinase-9/-2 in a rat model of cerebral ischemia-reperfusion injury. *Neurochem Res*. 2012;37(8):1820-1828.
26 Wang WQ, Liang XY, Fu D, et al. *Apocynum venetum* leaf attenuates myocardial ischemia/reperfusion injury by inhibiting oxidative stress. *Am J Chin Med*. 2015;43(1):71-85. https://doi.org/10.1142/S0192415X15500056
27 Lim SY, Bolster MB. Current approaches to osteoporosis treatment. *Curr Opin Rheumatol*. 2015;27(3):216-224. https://doi.org/10.1097/BOR.0000000000000169.
28 Honig S, Rajapakse CS, Chang G. Current treatment approaches to osteoporosis. *Bull Hosp Jt Dis*. 2013;71(3):184-188. https://doi.org/10.1097/bor.0000000000000169.
29 Sindel D. Osteoporosis: spotlight on current approaches to pharmacological treatment. *Turk J Phys Med Rehabil*. 2023;69(2):140-152. https://doi.org/10.5606/tftrd.2023.13054.
30 Robinson LJ, Yaroslavskiy BB, Griswold RD, et al. Estrogen inhibits RANKL-stimulated osteoclastic differentiation of human monocytes through estrogen and RANKL-regulated interaction of estrogen receptor-alpha with BCAR1 and TRAF6. *Exp Cell Res*. 2009;315(7):1287-1301. https://doi.org/10.1016/j.yexcr.2009.01.014.
31 Chen F, Ouyang Y, Ye T, et al. Estrogen inhibits RANKL-induced osteoclastic differentiation by increasing the expression of TRPV5 channel. *J Cell Biochem*. 2014;115(4):651-658. https://doi.org/10.1002/jcb.24700.
32 Banu J, Varela E, Fernandes G. Alternative therapies for the prevention and treatment of osteoporosis. *Nutr Rev*. 2012;70(1):22-40. https://doi.org/10.1111/j.1753-4887.2011.00451.x.
33 Zhang ND, Han T, Huang BK, et al. Traditional Chinese medicine formulas for the treatment of osteoporosis: implication for antiosteoporotic drug discovery. *J Ethnopharmacol*. 2016;189:61-80. https://doi.org/10.1016/j.jep.2016.05.025.
34 Ai C, Zou Y, Liu H, et al. Traditional Chinese herbal medicine for allergic diseases: a review. *Am J Chin Med*. 2023;51(4):779-806. https://doi.org/10.1142/S0192415X23500374.
35 Zeng P, Zhou H, Guo P, et al. Efficacy and safety of traditional Chinese herbal medicine in the treatment of threatened abortion: a protocol for systematic review and meta-analysis. *Medicine (Baltimore)*. 2021;100(5):e23288. https://doi.org/10.1097/MD.0000000000023288.
36 Yamatsu A, Yamashita Y, Maru I, et al. The improvement of sleep by oral intake of GABA and *Apocynum venetum* leaf extract. *J Nutr Sci Vitaminol (Tokyo)*. 2015;61(2):182-187. https://doi.org/10.3177/jnsv.61.182.
37 Ma YX, Chen SY. Observations on the anti-aging, antihypertensive and antihyperlipemic effect of *Apocynum venetum* leaf extract. *Chin J Integr Med*. 1989;9(6):335-337,323.
38 Reinhardt RA, Payne JB, Maze CA, et al. Influence of estrogen and osteopenia /osteoporosis on clinical periodontitis in postmenopausal women. *J Periodontol*. 1999;70(8):823-828. https://doi.org/10.1902/jop.1999.70.8.823.
39 Kusumbe AP, Ramasamy SK, Starsichova A, et al. Sample preparation for high-resolution 3D confocal imaging of mouse skeletal tissue. *Nat Protoc*. 2015;10(12):1904-1914. https://doi.org/10.1038/nprot.2015.125.